Electronic Supplementary Material (ESI) for Soft Matter.

Supplementary Information for Experimental Observation of the Asymmetric Instability of Intermediate-Reduced-Volume Vesicles in Extensional Flow

Joanna B. Dahl,[a] Vivek Narsimhan,[b] Bernardo Gouveia, [a] Sanjay Kumar,[a,c] Eric S. G. Shaqfeh,[d,e] and Susan J. Muller [*a]

[a.] *Department of Chemical and Biomolecular Engineering, University of California, Berkeley, Berkeley, CA, 94720-1460, USA. E-mail: muller2@berkeley.edu.*
[b.] *Department of Chemical Engineering, Massachusetts Institute of Technology, Cambridge, MA, 02139, USA.*
[c.] *Department of Bioengineering, University of California, Berkeley, Berkeley, CA, 94720-1762, USA.*
[d.] *Department of Chemical Engineering, Department of Mechanical Engineering, Stanford University, Stanford, CA, 94305, USA.*
[e.] *Institute of Computational and Mathematical Engineering, Stanford University, Stanford, CA, 94305, USA.*

Electroformation Protocol

Vesicles are prepared from a mixture of 1,2-dioleoyl-sn-glycero-3-phosphocholine (DOPC, Avanti Lipids) with fluorescent 1-oleoyl-2-{6-[(7-nitro-2-1,3-benzoxadiazol-4-yl)amino]hexanoyl}-sn-glycero-3-phosphocholine (NBD PC, ex/em 460/534 nm, Avanti Lipids). DOPC (1.68 mg/mL) and NBD PC (0.32 mg/mL) were mixed with chloroform for a total lipid concentration of 2 mg/mL. Fifteen microliters of the lipid solution is deposited on an indium tin oxide (ITO) slide (resistance 15-25 Ω, 25 x 25 x 1.1 mm, Delta Technologies). The slides are dried for 1-2 hours in a vacuum oven in the presence of desiccant to evaporate the solvent. A rubber gasket 1.6 mm thick is used as a spacer between two ITO slides. The electroformation cell is filled with a hydrating solution of 0.1 M sucrose (Sigma-Aldrich). Copper tape on opposite sides of the spacer are placed in contact with the conductive ITO surface and connected to a function generator (Agilent 33220A). A 3-hour electroformation program runs during which lipid layers peel off and form various aggregates, some of which are unilamellar vesicles. First a 10 Hz sine wave is linearly ramped from 0.05 V to 1.41 V over 30 minutes. Then a 20 Hz, 1.41 V_{pp} sine wave is applied for 2 hours. Finally, a 4.5 Hz, 2.12 V_{pp} square wave is applied for 30 minutes to promote release of vesicles attached to the slides.

Table S1: Bending Modulus Measurements

Measurement System	Bending modulus $\bar{\kappa} = \kappa/kT$	Surface Tension $\bar{\sigma} = \sigma R^2/\kappa$	Average Radius R [μm]	Correlation Cor($\bar{\kappa},\bar{\sigma}$)	Number of frames analyzed
Confocal Microscopy	14.0 ± 0.2	2 ± 1	8.20	-0.839	2500
Confocal Microscopy	15.7 ± 0.2	4 ± 1	7.30	-0.794	1740
Confocal Microscopy	13.9 ± 0.2	4.9 ± 0.7	6.56	-0.637	700
Fluorescence Microscopy	14.5 ± 0.4	143 ± 6	6.53	-0.854	491
Fluorescence Microscopy	15.0 ± 0.3	0.7 ± 0.8	8.25	-0.850	1901
Fluorescence Microscopy	16.4 ± 0.2	8.6 ± 0.8	15.4	-0.737	1766

Neglecting Gravity in Some Bending Modulus Measurements

The importance of gravity on vesicle thermal fluctuations can be estimated from Equation (53) in Henricksen and Ipsen (1). These authors established criteria in terms of a gravitational parameter (Bond number) $g_0 = \Delta\rho g R^4/\kappa$ which gives rise to perturbational corrections to the vesicle shape.

Criterion 1: The contact area between the vesicle and glass clover slip bottom is minimal. According to Equation 53 and assuming zero spontaneous curvature, this situation is met when $g_0 < (25/28)(12 + \bar{\sigma})$, where $\bar{\sigma} = \sigma R^2/\kappa$ is the reduced effective tension. The conditions of our experiment involved 1:1 dilution of vesicles in 0.1 M sucrose ($\rho = 1.01142$ g/mL) with 0.1 M glucose ($\rho = 1.00668$ g/mL), leading to density difference of $\Delta\rho = 2.37$ kg/m^3 between inside and outside the vesicles. Then using the values of $\bar{\kappa}, \bar{\sigma}$ and R measured for the three confocal microscopy measurements listed in Table S1, $g_0 = 1.832, 1.029, 0.754$, which is less than the quantity on the right side of the inequality for all three measurements. So for these measurements, the contact area is sufficiently small.

Criterion 2: The maximal relative gravitational correction to the vesicle fluctuation amplitudes is below an acceptable size, taken to be the experimental camera resolution. (Consult Figure 2 in Reference (1) below)

For our setup, the camera spatial resolution is 11.057 px/μm or 0.0904 μm/px, ~1% of the measured vesicle radius R. Looking at Figure 2, for $g_0 \sim 1$, the relative correction is less than 1% for all values of the effective surface tension. Therefore, we have justification to reasonably neglect gravitational effects for these three measurements.

Error Analysis

All reported values of the vesicle shape, bending modulus, and cross-slot extension rate are not directly measured but rather derived from detected contours of vesicles and seed particle motions in PIV. Thus starting from assumed uncertainties of the primary quantities measured (contour point pixel location, two-image intensity correlation function), we propagate the error

through analytical equations to determine the uncertainty of the derived quantity of interest. The general equations are given below, and details for each reported quantity are described in upcoming sections. These analyses are based on the principles of data reduction and error analysis discussed in Bevington and Robinson's book (2).

We assume that all measurements obey a Gaussian distribution with an unknown mean μ and standard deviation σ. This is a reasonable assumption because all experiments are independent and use the same instrumentation for a given measurement. From the probability density function of the presumed Gaussian distribution, expressions for the most probable value μ' and uncertainty of this value $\sigma_{\mu'}$ can be determined from N individual data measurements x_i and their individual uncertainties σ_i:

Equation S1

$$\mu' = \frac{\sum_i \left(x_i/\sigma_i^2\right)}{\sum_i \left(1/\sigma_i^2\right)} \quad \text{with} \quad \sigma_{\mu'}^2 = \sum_i \left[\sigma_i^2 \left(\frac{\partial \mu}{\partial x_i}\right)^2\right] = \frac{1}{\sum_i \left(1/\sigma_i^2\right)}$$

For measurements that share a common uncertainty $\sigma = \sigma_i$, these expressions simplify to

Equation S2

$$\mu' = \frac{1}{N}\sum_i x_i \quad \text{with} \quad \sigma_{\mu'}^2 = \frac{\sigma^2}{N}$$

In this case, the most probable value of the mean of the measurements is the sample average $\bar{x} \equiv \sum x_i/N$. The common uncertainty is estimated internally from the sample standard deviation $\sigma \cong s \equiv \sqrt{\sum \left(x_i - \bar{x}\right)^2/(N-1)}$.

Propagation of error through analytical expressions is determined from the chain rule. For a derived quantity $x = f(u,v)$ that depends on independent variables u and v, the variance of x, σ_x^2, is given by the error propagation equation:

Equation S3

$$\sigma_x^2 = \sigma_u^2 \left(\frac{\partial x}{\partial u}\right)^2 + \sigma_v^2 \left(\frac{\partial x}{\partial v}\right)^2 + \sigma_{uv}^2 \left(\frac{\partial x}{\partial u}\right)\left(\frac{\partial x}{\partial v}\right)$$

We assume that independent variables are uncorrelated so $\sigma_{uv}^2 = 0$. We report the uncertainty of the derived quantity to be the square root of its variance.

Vesicle Shape Measurement in Cross-slot

Due to thermal fluctuations present under elongation, vesicles are typically not exactly symmetric. Thus the vesicle contour is divided into left and right halves to be revolved independently about the axis of symmetry (Figure S1). The estimated surface area and volume

are the average of the left and right sides with the uncertainty estimated as half the discrepancy of the left and right sides (Figure S2(a)).

(a) Detected contour divided into left and right halves for shape analysis.

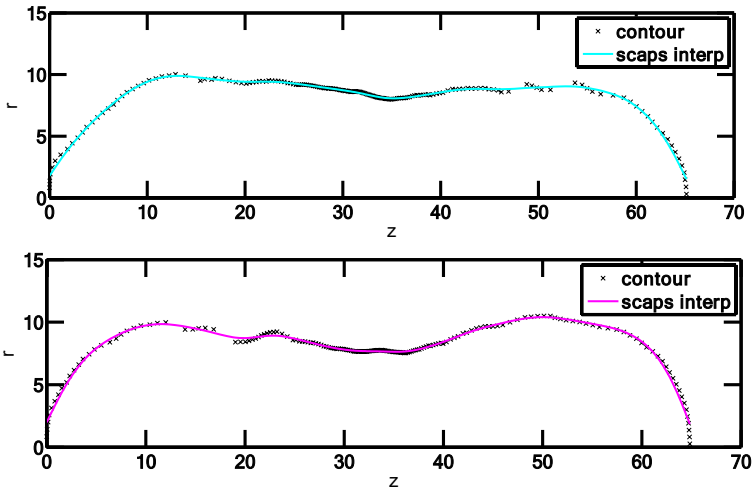

(b) Right and left cubic splines interpolated from the contour points using the Matlab cubic smoothing spline function `csaps` with a smoothing parameter of 0.1.

Figure S1. Vesicle shape detection for a single movie frame.

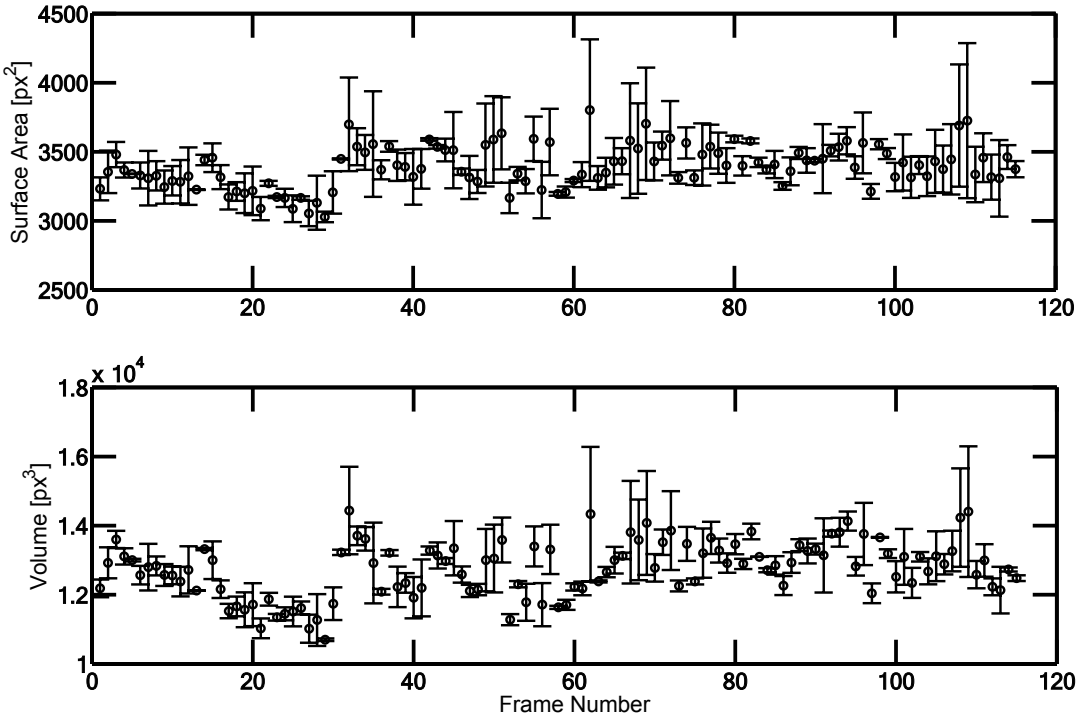

(a) Single frame surface area and volume values are the average of the left and right curve shapes of revolution. The error bars are the estimated uncertainty, taken to be one half the discrepancy between the left and right sides.

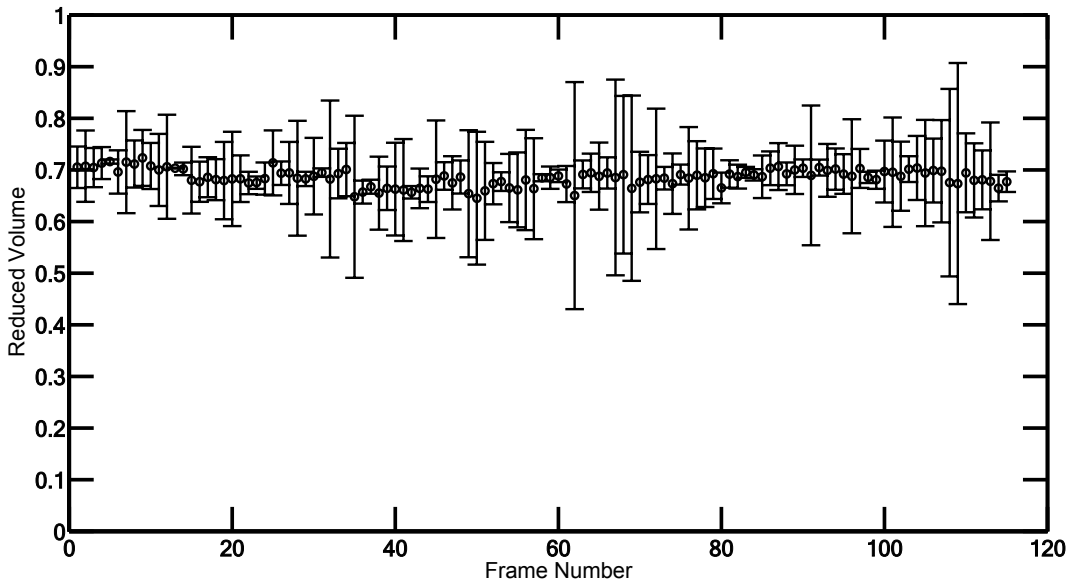

(b) Reduced volume measurement for individual frames calculated from surface area and volume measurements with uncertainties determined by propagation of error.

Figure S2. Vesicle shape measurement in the cross-slot for a stable, intermediate reduced volume vesicle. The final vesicle reduced volume was calculated to be $v = 0.7022 \pm 0.0008$, and the vesicle equivalent radius $R = \sqrt{A/4\pi} = 4.129 \pm 0.001$ μm.

Propagation of error in the measured vesicle surface area S_i and volume V_i for each movie frame i to the derived reduced volume $v_i = V_i/\left(4/3\pi R_0^3\right)$ where $R_0 = \sqrt{S_i/4\pi}$ is evaluated using Equation S3. The final reduced volume for the vesicle is the uncertainty-weighted average given in Equation S2.

Cross-slot rate of extension from PIV

Two experiments are performed at each flow rate. A least-square linear fitting procedure described in Chapter 4 of Bevington and Robinson (2) is employed to find the parameters a and b in $U = a\,r + b$ where $U = \sqrt{u^2 + v^2}$ and $r = \sqrt{x^2 + y^2}$. In perfectly planar extensional flow, $a = \dot{\varepsilon}$, i.e., the rate of extension and $b = 0$. The uncertainty in the velocity magnitude is assumed to dominate over the uncertainty of position r. We estimate the uncertainty of U by analyzing the spread in U values at a similar r location. The $U(r)$ data is separated into bins of width $\Delta r = 1$ μm, and the uncertainty of U, σ_U, is taken to be the maximum standard deviation of the binned U samples. For the 158-μm and 383-μm deep cross-slots, we have obtained a linear curve relating $\dot{\varepsilon}$ to the applied flow rate Q. In order to predict $\dot{\varepsilon}$ for flow rates at which PIV was not performed, a linear least-squares fit $\dot{\varepsilon} = a\,Q + b$ is used. The uncertainty of interpolation or extrapolation from the $\dot{\varepsilon}(Q)$ curve with N data points is estimated from the linear fit according to Equation 6.15 of Bevington and Robinson (2):

Equation S4

$$\sigma_{\dot{\varepsilon}}^2 \cong s^2 = \frac{1}{N-2}\sum_{i=1}^{N}\left(\dot{\varepsilon}_i - aQ_i - b\right)^2$$

For the approximately 150-μm-deep cross-slot, the $\dot{\varepsilon}$ value is determined from PIV analysis of vesicles steadily flowing through the cross-slot at 350 μL/hr. The final value is the uncertainty-weighted average of two movies of 70 and 500 frames. The result is $\dot{\varepsilon}_{350\,\mu L/hr} = 0.3676 \pm 0.0051$ s^{-1}. For other flow rates used in that device and included in the stability diagram (300, 400, 500 μL/hr), we proportionally modify strain rate with flow rate:

$$\dot{\varepsilon}(Q) = \dot{\varepsilon}_{350\,\mu L/hr} \cdot \frac{Q}{350\ \mu L/hr}$$

and use the same uncertainty, $\sigma_{\dot{\varepsilon}} = 0.0051\ \mathrm{s}^{-1}$.

Table S2: Stability Diagram Points and Uncertainties

All points included in the stability diagram are reported below with their individual uncertainties.

Reduced volume $v = 3V/4\pi a^3$	**Reduced volume uncertainty** σ_v	**Capillary number** $Ca = \mu\dot{\varepsilon}a^3/\kappa$	**Capillary number uncertainty** σ_{Ca}	**Status**
0.8841	0.0008	9.2	0.3	stable
0.7022	0.0008	6.8	0.2	stable
0.9116	0.0003	21.2	0.6	stable
0.7730	0.0002	57	2	stable
0.775	0.001	13.2	0.4	stable
0.7546	0.0003	260	8	stable
0.9025	0.0002	64	2	stable
0.8597	0.0002	125	3	stable
0.8422	0.0006	43	1	stable
0.8921	0.0002	18.7	0.5	stable
0.8762	0.0003	39	1	stable
0.9433	0.0005	15.3	0.4	stable
0.9431	0.0005	35	1	stable
0.9075	0.0002	94	3	stable
0.8548	0.0001	315	9	stable
0.8376	0.0006	3.8	0.1	stable
0.8595	0.0005	15.8	0.4	stable
0.8767	0.0003	3.3	0.1	stable
0.8051	0.0003	94	3	stable
0.9285		10.4		stable
0.9015		146		stable

0.8735		51.3		stable
0.8173		89.6		stable
0.9120		78.7		stable
0.9210		32.5		stable
0.8960		143		stable
0.606	0.012	92	3	unstable
0.611	0.014	74	2	unstable
0.6171	0.0002	89	3	unstable
0.654	0.002	95	3	unstable
0.63	0.03	71	3	unstable
0.675	0.004	72	2	unstable
0.54	0.02	47	2	unstable
0.68	0.05	27.0	0.9	unst. less certainty
0.65	0.01	134	4	unst. less certainty
0.60	0.04	10.0	0.4	unst. less certainty
0.55	0.06	11.1	0.4	unst. less certainty
0.64	0.01	7.2	0.2	unst. less certainty
0.64	0.03	152	5	unst. less certainty

Supplementary Movies

Movie 1: Stable vesicle

This vesicle is stable in an extensional flow field with $\dot{\varepsilon} = 0.317$ s^{-1}. Membrane fluctuations are visible even though the vesicle is elongated. The relatively large reduced volume of $v = 0.8595 \pm 0.0005$ and capillary number of $Ca = 15.77 \pm 0.44$ place this vesicle well within the stable region. Scale bar is 20 μm. Cross-slot dimensions: 2 mm wide, 383 μm deep.

Movie 2: Unstable vesicle

An intermediate-reduced-volume vesicle is brought to the stagnation point by adjusting the height and therefore pressure difference between the two outlet reservoirs. After a few seconds, the vesicle breaks up asymmetrically in the extensional flow with a strain rate of $\dot{\varepsilon} = 0.368$ s^{-1}. The tether elongates and pearls as the bulbous ends become more spherical. The reduced volume before the onset of the instability is measured to be $v = 0.6061 \pm 0.0120$, and the capillary number is $Ca = 78.60 \pm 2.56$. Scale bar is 20 μm. Cross-slot dimensions: 2 mm wide, approximately 150 μm deep.

Movie 3: Stable vesicle close to stability boundary

During the 20 seconds this vesicle is trapped near the stagnation point with an extensional strain rate of $\dot{\varepsilon} = 0.420$ s^{-1}, the vesicle remains stable. The reduced volume and capillary number are $v = 0.7022 \pm 0.0008$ and $Ca = 6.825 \pm 0.202$, putting this vesicle in close proximity to, and

on the stable side of, the predicted stability curve. Scale bar is 20 μm. Cross-slot dimensions: 2 mm wide, approximately 150 μm.

References

1. Henriksen JR, Ipsen JH. 2002. Thermal undulations of quasi-spherical vesicles stabilized by gravity. *Eur. Phys. J. E*. 9(4):365–74
2. Bevington PR, Robinson DK. 2003. *Data Reduction and Error Analysis for the Physical Sciences*. New York: McGraw-Hill. Third ed.